

Uniform convergent scheme for strongly anisotropic diffusion equations with closed field lines

Yihong Wang ^{*}Wenjun Ying [†]Min Tang [‡]

November 1, 2016

Abstract

In magnetized plasma, the magnetic field confines particles around field lines. The ratio between the intensity of the parallel and perpendicular viscosity or heat conduction may reach the order of 10^{12} . When the magnetic fields have closed field lines and form a “magnetic island”, the convergence order of most known schemes depends on the anisotropy strength. In this paper, by integration of the original differential equation along each closed field line, we introduce a simple but very efficient asymptotic preserving reformulation, which yields uniform convergence with respect to the anisotropy strength. Only slight modification to the original code is required and neither change of coordinates nor mesh adaptation is needed. Numerical examples demonstrating the performance of the new scheme are presented.

Key words: Anisotropic diffusion; Asymptotic Preserving; Uniform convergence; Field line integration.

1 Introduction

Anisotropic diffusion is encountered in many fields such as heat conduction in magnetized plasma [8], flows in porous media [2], image processing or oceanic flows [9, 22]. We are particularly interested in the anisotropic diffusion in magnetized plasmas. It has extremely anisotropic diffusion tensors of heat conduction in fusion plasmas, where the particles are confined by the magnetic field and the particle diffusion is much faster along the field lines than in the perpendicular direction [8].

In magnetized plasma, magnetic field lines can be open or closed. The region that has closed field lines inside is called a “magnetic island”. The field lines outside the region are open. Plasma transportation across these closed field lines depends on the perpendicular diffusion coefficients. Small diffusion coefficients in the perpendicular direction lead to plasma confinement. The closed field lines relate to the important physical process “magnetic reconnection” and can appear as a consequence of instabilities or external perturbations.

^{*}Institute of natural sciences and department of mathematics, Shanghai Jiao Tong University, Shanghai, 200240, China.

[†]Institute of natural sciences and department of mathematics, Shanghai Jiao Tong University, Shanghai, 200240, China.

[‡]Institute of natural sciences and department of mathematics, Shanghai Jiao Tong University, Shanghai, 200240, China.

The problem under consideration is the following two-dimensional diffusion equation with anisotropic diffusivity:

$$\begin{cases} -\nabla \cdot (A \nabla u^\epsilon) = f, & \text{in } \Omega, \\ u^\epsilon = g, & \text{on } \partial\Omega, \end{cases} \quad (1)$$

where $\Omega \subset \mathbb{R}^2$ is a bounded domain with boundary $\partial\Omega$. The diffusion tensor is given by

$$A(x, y) = \begin{pmatrix} \cos \theta & -\sin \theta \\ \sin \theta & \cos \theta \end{pmatrix} \begin{pmatrix} 1/\epsilon & 0 \\ 0 & \alpha \end{pmatrix} \begin{pmatrix} \cos \theta & \sin \theta \\ -\sin \theta & \cos \theta \end{pmatrix}, \quad (2)$$

where α is $O(1)$ and the parameter $0 < \epsilon < 1$ can be very small. All coefficients α , ϵ and θ may depend on space. The direction of the anisotropy or the magnetic field line is given by a unit vector field $\mathbf{b} = (\cos \theta, \sin \theta)^T$, while α and $1/\epsilon$ are respectively the perpendicular and parallel diffusion coefficients. The problem becomes highly anisotropic when $\epsilon \ll 1$.

Numerical simulations for anisotropic diffusion problems have been addressed by a lot of researchers and engineers; see the review in [12]. Methods used today include finite volume method [20, 21, 24], finite difference method [8], mimetic finite difference method [14], discontinuous Galerkin method [1, 7], finite element method [10, 13, 15, 19] and so on. These methods are usually efficient for a selected range of ϵ but loss convergence when $\epsilon \ll h$ (h is the mesh size).

A field-aligned coordinate system is usually employed for plasma simulations. However, it may run into problems when there are magnetic re-connections or highly fluctuating field directions. Schemes with non-aligned meshes in case of varying anisotropy have been studied as well, for instance [8, 10, 11] and the references there in. Since the numerical errors in the direction parallel to the magnetic field may have significant effect on the perpendicular direction, several difficulties arise for strongly anisotropic diffusion problems with non-aligned meshes, which include pollution on the perpendicular direction by the parallel diffusion and loss of convergence, etc [8].

In this paper, we are interested in the case when the magnetic field exhibits closed field lines. First, due to the closed field lines, numerical discretizations of the original problem using magnetic field aligned coordinates lead to very badly conditioned systems when ϵ becomes small. The limiting model is not well-posed and admits infinitely many solutions [18], as adding any function constant in the region covered by closed field lines keeps a solution to the limiting model. Second, when non-aligned coordinates are used, most known schemes loss convergence when $\epsilon \rightarrow 0$ [8, 10, 11]. If the field line directions are taken into account in the numerical discretization, uniform convergence can be achieved when the closed field line is symmetric, but all schemes in [8, 10, 11] fail to converge when $\epsilon \ll h$ in the tilted closed field line case.

That the scheme convergence is independent of ϵ can be considered as an Asymptotic preserving (AP) property. Asymptotic preserving (AP) methods for strongly anisotropic diffusion have been studied in a series paper by Degond et.al [3, 4, 5, 6, 16, 17]. AP schemes have the advantage that the condition number does not scale with the anisotropy, when using Neumann or periodic boundary conditions, thus can deal with all ϵ ranging from $O(1)$ to very small. The main idea in [3, 4, 5, 6, 16, 17] are based on macro-micro decomposition, and reformulate the original equation into a system that keeps well-posed when $\epsilon \rightarrow 0$. For the closed field line case, Narski and Ottaviani [18] developed a uniform convergent scheme by introducing a penalty stabilization term, where a tuning parameter is needed.

In this paper, we propose a different approach, which is simple and easily extendable. The main idea is that we cut each closed field line at some point (x_0, y_0) , which is treated as the begin and end points of the cut field line. Then instead of discretizing the equation at the point (x_0, y_0) locally, we work

with integration of the differential equation along the cut field line. By using continuity conditions at the cutting point (x_0, y_0) , the singular $1/\epsilon$ terms disappear, so that the reformulated problem becomes well-posed.

The idea is inspired by the AP method developed in [23] for the strongly anisotropic diffusion equation with Neumann boundary conditions. After replacing one of the Neumann boundary condition by integration of the original differential equation along the field line, an equivalent new system that is well-posed in the limit $\epsilon \rightarrow 0$ can be constructed. Any numerical discretization based on this new system has uniform convergence with respect to ϵ .

The main advantage of the field line integration approach is that: 1) uniform convergence is numerically achieved even for the tilted closed field line case; 2) only slight modification to the original code is needed, which make it attractable for engineers; 3) no tuning parameter is introduced; 4) no coordinate change or mesh adaptation is required.

The paper is organized as follows. In section 2, we illustrate the idea of the reformulation. Numerical discretizations are given in Section 3, where nine point finite difference method (FDM) is used for the reformulated system. Several numerical examples are presented in section 4, which show the uniform convergence of the scheme with respect to the anisotropy. Finally we conclude with some discussions in section 5.

2 The Asymptotic Preserving Reformulation

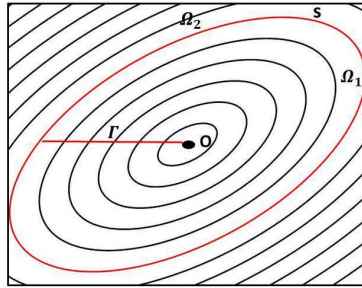


Figure 1: Closed field lines.

Let $\Omega = (-a, a) \times (-b, b)$ be the computational domain. Assume it can be partitioned into two non-overlapping open subdomains Ω_1 and Ω_2 by a separatrix S such that $\Omega = \Omega_1 \cup \Omega_2 \cup S$. All field lines in Ω_1 are closed and those in Ω_2 are open.

We first discuss about the subdomain Ω_2 with open field lines. In the open field line subdomain Ω_2 , Eqn (1) remains the same, any scheme in [8, 10, 11] can be applied. Whether a field line ℓ is considered as an open or closed field line depends on whether it intersects with the boundary $\partial\Omega$ or not. If $\partial\Omega \cap \ell = \emptyset$, then ℓ is a closed field line. If $\partial\Omega \cap \ell \neq \emptyset$, then ℓ is open. The region inside S is a "magnetic island". Outside S , the field lines are open (see Figure 1 for an illustration).

In the subsequent part, we will construct an equivalent system in Ω_1 ($\Omega_1 \cup S$). To illustrate the idea, we use the notations in Figure 1. It is important to note that when there are closed field lines, one can

find a singular point inside Ω_1 where $\cos \theta$ and $\sin \theta$ have no definition. It is considered as the center of the "magnetic island". Suppose $O(0,0)$ is the center of the "magnetic island" and ℓ ($\ell \in \Omega_1 \cup S$) is a close field line.

2.1 An interface problem

Let $\mathbf{b} = (\cos \theta, \sin \theta)^T$, $\mathbf{b}_\perp = (-\sin \theta, \cos \theta)^T$, Eqn (1) can be written as

$$-(\mathbf{b} \cdot \nabla) \left(\frac{1}{\epsilon} \mathbf{b} \cdot \nabla u^\epsilon \right) - (\nabla \cdot \mathbf{b}) \left(\frac{1}{\epsilon} \mathbf{b} \cdot \nabla u^\epsilon \right) - \nabla \cdot (\alpha \mathbf{b}_\perp (\mathbf{b}_\perp \cdot \nabla u^\epsilon)) = f. \quad (3)$$

We can pick any \mathbf{b} -field line ℓ and parameterize it by the arc length s . Accordingly, ∂_s will denote the derivative along the line ℓ , i.e. $\partial_s = \mathbf{b} \cdot \nabla$. Then, Eqn (3) can be written as

$$-\partial_s \left(\frac{1}{\epsilon} \partial_s u^\epsilon \right) - (\nabla \cdot \mathbf{b}) \frac{1}{\epsilon} \partial_s u^\epsilon - \nabla \cdot (\alpha \mathbf{b}_\perp (\mathbf{b}_\perp \cdot \nabla u^\epsilon)) = f. \quad (4)$$

In the strong anisotropic diffusion limit as $\epsilon \rightarrow 0$, (4) yields

$$-\partial_s^2 u^0 - (\nabla \cdot \mathbf{b}) \partial_s u^0 = 0. \quad (5)$$

If ℓ is closed, any function that is constant along ℓ satisfies (5). There is no uniqueness of the solution to the limiting model, which explains the ill-posedness when a field-aligned coordinate is used in the numerical discretization.

We cut ℓ at a point (x_0, y_0) . Starting from (x_0, y_0) and following the direction \mathbf{b} , we can determine (x_{0+}, y_{0+}) and (x_{0-}, y_{0-}) , which are respectively the start and end point of ℓ . Since ℓ is closed,

$$(x_{0+}, y_{0+}) = (x_{0-}, y_{0-}) = (x_0, y_0). \quad (6)$$

When $A(x, y)$ is continuous, the solution to (1) belongs to $C^1(\Omega)$, thus both u^ϵ and ∇u^ϵ are continuous at (x_0, y_0) . However, this regularity requirement is not necessarily true for the limiting equation (5). Since s is the arc length, $s = 0$ corresponds to (x_{0+}, y_{0+}) and $s = L_\ell$ with L_ℓ being the length of ℓ corresponds to (x_{0-}, y_{0-}) . Eqn (5) holds at all points on ℓ , which indicates that

$$u^0|_{s=0} = u^0|_{s=L_\ell}, \quad \partial_s u^0|_{s=0} = \partial_s u^0|_{s=L_\ell}.$$

Therefore, due to the regularity requirement, the following connection conditions

$$u_+^\epsilon = u_-^\epsilon, \quad \frac{1}{\epsilon} \mathbf{t} \cdot \mathbf{b} (\mathbf{b} \cdot \nabla u_+^\epsilon) + \alpha \mathbf{t} \cdot \mathbf{b}_\perp (\mathbf{b}_\perp \cdot \nabla u_+^\epsilon) = \frac{1}{\epsilon} \mathbf{t} \cdot \mathbf{b} (\mathbf{b} \cdot \nabla u_-^\epsilon) + \alpha \mathbf{t} \cdot \mathbf{b}_\perp (\mathbf{b}_\perp \cdot \nabla u_-^\epsilon), \quad (7)$$

should be satisfied independent of ϵ . Here $u_+^\epsilon = u^\epsilon(x_{0+}, y_{0+})$, $u_-^\epsilon = u^\epsilon(x_{0-}, y_{0-})$ and (7) can be written as

$$u^\epsilon(x_{0+}, y_{0+}) = u^\epsilon(x_{0-}, y_{0-}), \quad \mathbf{t} \cdot A(x_0, y_0) \nabla u^\epsilon(x_{0+}, y_{0+}) = \mathbf{t} \cdot A(x_0, y_0) \nabla u^\epsilon(x_{0-}, y_{0-}),$$

where \mathbf{t} is the tangent direction of the field line across (x_0, y_0) .

On each closed field line, we choose a cutting point. To describe the calculation better, we can suppose all cutting points are on the negative X axis. Let Γ be the set of all cutting points (see Figure 1). Then we have the following interface problem:

$$\begin{cases} -(\mathbf{b} \cdot \nabla) \left(\frac{1}{\epsilon} \mathbf{b} \cdot \nabla u^\epsilon \right) - (\nabla \cdot \mathbf{b}) \left(\frac{1}{\epsilon} \mathbf{b} \cdot \nabla u^\epsilon \right) - \nabla \cdot (\alpha \mathbf{b}_\perp (\mathbf{b}_\perp \cdot \nabla u^\epsilon)) = f, & \text{on } \Omega_1 \setminus \Gamma, \\ u^\epsilon(x_{0+}, y_{0+}) = u^\epsilon(x_{0-}, y_{0-}), & \text{for } \forall (x_0, y_0) \in \Gamma, \\ \mathbf{t} \cdot A(x_0, y_0) \nabla u^\epsilon(x_{0+}, y_{0+}) = \mathbf{t} \cdot A(x_0, y_0) \nabla u^\epsilon(x_{0-}, y_{0-}), & \text{for } \forall (x_0, y_0) \in \Gamma. \end{cases} \quad (8)$$

Remark 2.1 If u^ϵ is the solution to the original problem (1), it satisfies the interface problem (8). On the other hand, it is easy to check that when $u^\epsilon \in C^1(\Omega)$ and satisfies the interface problem (8), it is a solution to the original problem (1).

2.2 Reformulation of the interface problem

By similar argument as in section 2.1, the interface problem (8) is ill-posed when $\epsilon \rightarrow 0$. However, we can replace the continuity of the derivatives at the interface points by integration of the equation along the field lines, and derive an equivalent system that is well-posed when $\epsilon \rightarrow 0$. The details are as follows.

First of all, we introduce a function E defined on Ω_2 . Assume the field line $\ell \subset \Omega_2$ starts and ends at (x_0, y_0) . The function E solves on the field line ℓ the differential equation

$$\partial_s E = (\nabla \cdot \mathbf{b})E, \quad E(0) = 1. \quad (9)$$

The solution to (9) is $E(s) = e^{\int_0^s \nabla \cdot \mathbf{b} ds'}$. The following lemma indicates that if the limiting solution u^0 exists, $E(L_\ell) = E(0) = 1$. Here, L_ℓ is the arc length of the field line ℓ .

Lemma 2.2 If there exists a function $v(x, y) \in C^2(\ell)$ such that $\mathbf{b} = \frac{1}{|\nabla v|}(-v_y, v_x)^T$, $\int_0^{L_\ell} \nabla \cdot \mathbf{b} ds = 0$.

Proof. : Let $\mathbf{b} = (\dot{x}(t), \dot{y}(t))^T$ with

$$\dot{x}(t) = \frac{-v_y(x(t), y(t))}{|\nabla v|}, \quad \dot{y}(t) = \frac{v_x(x(t), y(t))}{|\nabla v|},$$

$t = t_0$ correspond to $s = 0$ and $t = t_l$ correspond to $s = L_\ell$. Therefore, $t = t_0$ and $t = t_l$ correspond to the same point in Ω and $v_x|_{t=t_0} = v_x|_{t=t_l}$, $v_y|_{t=t_0} = v_y|_{t=t_l}$. Besides from $\dot{x}(t)^2 + \dot{y}(t)^2 = 1$, $ds = dt$. Then

$$\begin{aligned} \int_0^{L_\ell} \nabla \cdot \mathbf{b} ds &= \int_{t_0}^{t_l} \partial_x \left(\frac{-v_y}{|\nabla v|} \right) + \partial_y \left(\frac{v_x}{|\nabla v|} \right) dt \\ &= \int_{t_0}^{t_l} \frac{-v_x^2 v_{xy} - v_x v_y v_{yy} + v_y^2 v_{xy} + v_x v_y v_{xx}}{(v_x^2 + v_y^2)^{3/2}} dt \\ &= \int_{t_0}^{t_l} - \frac{(v_y v_{xy} + v_x v_{xx}) \dot{x}(t) + (v_x v_{xy} + v_y v_{yy}) \dot{y}(t)}{v_x^2 + v_y^2} dt \\ &= \int_{t_0}^{t_l} - \frac{\frac{1}{2}(v_x^2 + v_y^2)_x \dot{x}(t) + \frac{1}{2}(v_x^2 + v_y^2)_y \dot{y}(t)}{v_x^2 + v_y^2} dt. \\ &= \int_{t_0}^{t_l} - \frac{d}{dt} \left\{ \frac{\ln(v_x^2 + v_y^2)}{2} \right\} dt = 0. \end{aligned}$$

□

If the limiting solution u^0 exists, from (5), it satisfies $\mathbf{b} \cdot \nabla u^0 = 0$ along the closed field lines. Then the vector field \mathbf{b} can be determined by $\mathbf{b} = \frac{1}{|\nabla u^0|}(-u_y^0, u_x^0)^T$. The above Lemma gives $E(0) = E(L_\ell) = 1$. It is important to note that this property does not rely on the value of ϵ .

We multiply both sides of (4) by E and combine the two singular $O(1/\epsilon)$ terms to get

$$-\partial_s \left(E \frac{1}{\epsilon} \partial_s u^\epsilon \right) - E \nabla \cdot (\alpha \mathbf{b}_\perp (\mathbf{b}_\perp \cdot \nabla u^\epsilon)) = E f. \quad (10)$$

Then integrating (10) over ℓ gives us

$$-E \frac{1}{\epsilon} \partial_s u^\epsilon \Big|_{s=0}^{s=L_\ell} - \int_0^{L_\ell} E \nabla \cdot (\alpha \mathbf{b}_\perp (\mathbf{b}_\perp \cdot \nabla u^\epsilon)) ds = \int_0^{L_\ell} E f ds. \quad (11)$$

From $\partial_s u^\epsilon|_{s=0} = \partial_s u^\epsilon|_{s=L_\ell}$, and $E(0) = E(L_\ell) = 1$, let S_Γ be the set of all closed field lines that satisfy $\ell(L_\ell) \in \Gamma$, (8) can then be reformulated as

$$\begin{cases} -(\mathbf{b} \cdot \nabla) \left(\frac{1}{\epsilon} \mathbf{b} \cdot \nabla u^\epsilon \right) - (\nabla \cdot \mathbf{b}) \left(\frac{1}{\epsilon} \mathbf{b} \cdot \nabla u^\epsilon \right) - \nabla \cdot (\alpha \mathbf{b}_\perp (\mathbf{b}_\perp \cdot \nabla u^\epsilon)) = f, & \text{on } \Omega_1, \\ u^\epsilon(x_{0+}, y_{0+}) = u^\epsilon(x_{0-}, y_{0-}), & \text{for } \forall (x_0, y_0) \in \Gamma, \\ \int_0^{L_\ell} E \left(\nabla \cdot (\alpha \mathbf{b}_\perp (\mathbf{b}_\perp \cdot \nabla u^\epsilon)) + f \right) ds = 0 & \text{for } \forall \ell \in S_\Gamma. \end{cases} \quad (12)$$

It is easy to check that when ϵ is finite, the above system is equivalent to the interface problem (8). The advantage of the reformulation (12) is when $\epsilon \rightarrow 0$, its leading order gives

$$\begin{cases} -\partial_s^2 u^0 - (\nabla \cdot \mathbf{b}) \partial_s u^0 = 0, & \text{in } \Omega_1, \\ u^0|_{s=0} = u^0|_{s=L_\ell}, & \text{on } \Gamma, \\ \int_0^{L_\ell} E \left(\nabla \cdot (\alpha \mathbf{b}_\perp (\mathbf{b}_\perp \cdot \nabla u^0)) + f \right) ds = 0, & \text{for } \forall \ell \in S_\Gamma. \end{cases} \quad (13)$$

The first two equations in (13) indicate that u^0 is constant along ℓ while the third equation determines the constant.

In summary, combining the equation on Ω_2 with (12), we get the asymptotic preserving reformulation for (1) on the whole computational domain such that

$$\begin{cases} -(\mathbf{b} \cdot \nabla) \left(\frac{1}{\epsilon} \mathbf{b} \cdot \nabla u^\epsilon \right) - (\nabla \cdot \mathbf{b}) \left(\frac{1}{\epsilon} \mathbf{b} \cdot \nabla u^\epsilon \right) - \nabla \cdot (\alpha \mathbf{b}_\perp (\mathbf{b}_\perp \cdot \nabla u^\epsilon)) = f, & \text{on } \Omega \setminus \Gamma, \\ u^\epsilon(x_{0+}, y_{0+}) = u^\epsilon(x_{0-}, y_{0-}), & \text{on } \Gamma, \\ \int_0^{L_\ell} E \left(\nabla \cdot (\alpha \mathbf{b}_\perp (\mathbf{b}_\perp \cdot \nabla u^\epsilon)) + f \right) ds = 0, & \text{on } \ell \in S_\Gamma, \\ u^\epsilon = g, & \text{on } \partial\Omega, \end{cases} \quad (14)$$

with E defined as in (9).

Remark 2.3 Although \mathbf{b} is continuous, $\nabla \cdot \mathbf{b}$ may have jumps. This is always the case for “magnetic islands”. Examples can be found in our numerical examples in section 4. Then, E are only C^0 but not C^1 . To get a good approximation of the integration in (14), we have to take into account the discontinuities in $\nabla \cdot \mathbf{b}$.

3 Numerical Discretization

Suppose the rectangle domain $\Omega = (-a, a) \times (-b, b)$ is partitioned into a uniform Cartesian grid with nodes

$$\mathbf{z}_{i,j} = (x_i, y_j), \quad i = 0, \pm 1, \dots, \pm I; \quad j = 0, \pm 1, \dots, \pm J.$$

Here, I and J are two positive integers, $x_i = ih_x$ and $y_j = jh_y$ with $h_x = a/I$, $h_y = b/J$.

The major difficulty in discretizing the system (14) lies in the integration of the differential equations along closed field lines. First we explain details on numerical calculation of closed field lines and selection of the quadrature points for numerical integration. Then we present the scheme that is used in our numerical tests. However, the reformulation does not rely on the specific discretization. Other schemes can be applied as well.

3.1 Determine the closed field lines and the quadrature

Determine the open field lines: Based on the vector field $\mathbf{b} = (\cos \theta, \sin \theta)^T$, we can determine the field line by the following nonlinear ODE system:

$$\begin{cases} \dot{x}(t) = \cos \theta(x(t), y(t)), & x(0) = x_0, \\ \dot{y}(t) = \sin \theta(x(t), y(t)), & y(0) = y_0. \end{cases} \quad (15)$$

To get the field line ℓ , we use a high order Runge-Kutta method with small time step to solve the above system. Numerically, we can successively obtain the discrete points $\{(x_0, y_0), (x_1, y_1), \dots, (x_n, y_n)\}$ which form a discretization of the corresponding field line. If the field line is open, the calculations stop when x_n or y_n exceeds the boundary.

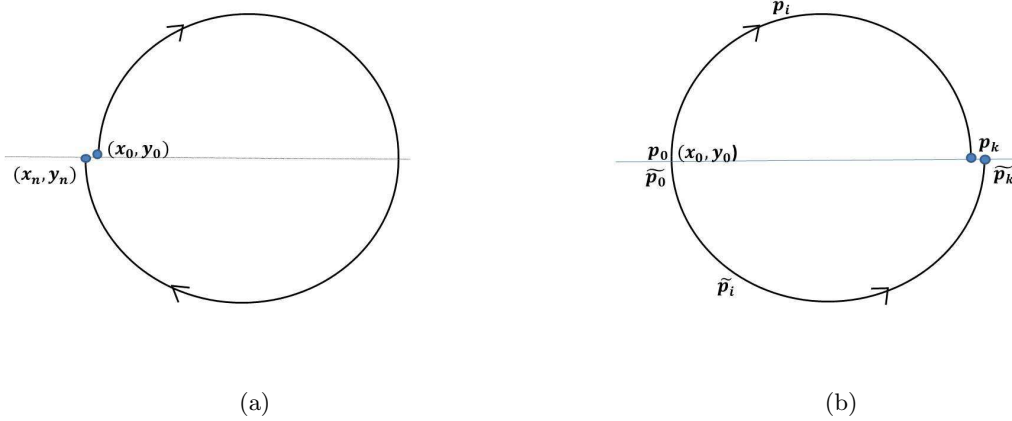


Figure 2: (a). Closed field line is solved by “Method One”. (b). Closed field line is solved by “Method Two”.

Determine the closed field lines: In the case of closed field lines, due to numerical errors, the approximated field line is not necessarily closed, the calculation stops when $(x_n, y_n) \in O((x_0, y_0), \delta)$ with $\delta = \min\{h_x, h_y\}$. However, when h_x, h_y become small, there may exist no such (x_n, y_n) , see Figure 2 (a). In this case, the start and end points can not be considered as identical and the connection conditions in (7) can be violated. We call this approximation as “Method One”. To avoid this problem, we can determine a closed field line by solving the following two systems simultaneously with the same time step

$$\begin{cases} \dot{x}(t) = \cos \theta(x(t), y(t)), & x(0) = x_0 \\ \dot{y}(t) = \sin \theta(x(t), y(t)), & y(0) = y_0 \end{cases} \quad \text{and} \quad \begin{cases} \dot{x}(t) = -\cos \theta(x(t), y(t)), & x(0) = x_0 \\ \dot{y}(t) = -\sin \theta(x(t), y(t)), & y(0) = y_0 \end{cases}. \quad (16)$$

The first system in (16) yields a sequence of points on ℓ , we denote them by p_k ($k = 0, 1, \dots$). The second system yields another sequence \tilde{p}_k ($k = 0, 1, \dots$). Then the calculations stop when $p_k \in O(\tilde{p}_k, \delta)$ with $\delta = \min\{h_x, h_y\}$ or when $\{|p_{k-1} - \tilde{p}_{k-1}|, |p_{k+1} - \tilde{p}_{k+1}|\} > |p_k - \tilde{p}_k|$, see Figure 2 (b). So the points $\{p_0, p_1, \dots, p_k, \tilde{p}_k, \tilde{p}_{k-1}, \dots, \tilde{p}_0\}$ form a discretization of the corresponding field line (called it “Method Two”). Since we will replace the local discretization at the point p_0 (\tilde{p}_0) by the field line integration, the start and end points are identical for method two, so that the interface conditions in (7) remain valid. We will see from the numerical examples that the results are different for these two different ways of determining the field lines.

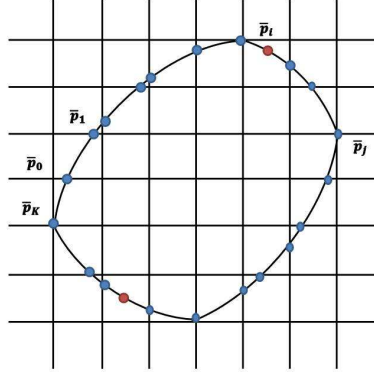


Figure 3: Notations of the quadrature points along the closed field line ℓ . Here those points on cell edges are denoted by \bar{p}_k ($k = 2, 3, 4, \dots, K$) and the two star points inside the cell are the discontinuities of $\nabla \cdot \mathbf{b}$.

Determine the quadrature points: The numerical quadrature points are given by interpolation. To simplify some of the notations as well as to make the discussions clearer, we use the field line and notations in Figure 3 as an example.

In order to evaluate the integral along the field line ℓ , the quadrature points are determined by the intersection points of ℓ with those cell edges that are parallel to the x axis or y axis. We denote the intersection points by (x_i, \bar{y}_i) or (\bar{x}_j, y_j) . They are numerically determined by linear interpolation of the discrete points p_k . It is important to note that $\nabla \cdot \mathbf{b}$ can have jumps. To get a good approximation of E in (9) as well as the integration in (14), the discontinuities of $\nabla \cdot \mathbf{b}$ on the field line should be included in the quadrature set. We denote by $S_\ell = \{\bar{p}_k, k = 0, 1, 2 \dots K_\ell\}$ the set of all quadrature points on the field line ℓ .

3.2 9-Point FDM

For all those grid points inside the computational domain $\Omega \setminus \Gamma$, we use the classical 9-Point finite difference method (FDM) to discretize the first equation in (14). First of all, we use $v_{i\pm 1/2, j} \approx v(x_{i\pm 1/2}, y_j)$, $v_{i, j\pm 1/2} \approx v(x_i, y_{j\pm 1/2})$ to approximate a general function v . The standard centered

difference approximations read

$$\begin{aligned}
\frac{\partial u^\epsilon}{\partial x} \Big|_{i\pm 1/2,j} &\approx \frac{u_{i\pm 1,j}^\epsilon - u_{i,j}^\epsilon}{\pm h_x}, & \frac{\partial u^\epsilon}{\partial y} \Big|_{i,j\pm 1/2} &\approx \frac{u_{i,j\pm 1}^\epsilon - u_{i,j}^\epsilon}{\pm h_y}, \\
\frac{\partial u^\epsilon}{\partial y} \Big|_{i\pm 1/2,j} &\approx \frac{u_{i\pm 1/2,j+1}^\epsilon - u_{i\pm 1/2,j-1}^\epsilon}{2h_y} \approx \frac{u_{i\pm 1,j+1}^\epsilon + u_{i,j+1}^\epsilon - u_{i,j-1}^\epsilon - u_{i\pm 1,j-1}^\epsilon}{4h_y}, \\
\frac{\partial u^\epsilon}{\partial x} \Big|_{i,j\pm 1/2} &\approx \frac{u_{i+1,j\pm 1/2}^\epsilon - u_{i-1,j\pm 1/2}^\epsilon}{2h_x} \approx \frac{u_{i+1,j\pm 1}^\epsilon + u_{i+1,j}^\epsilon - u_{i-1,j}^\epsilon - u_{i-1,j\pm 1}^\epsilon}{4h_x}.
\end{aligned} \tag{17}$$

Let $Q = (Q^{(1)}, Q^{(2)}) = A\nabla u^\epsilon$. We approximate the diffusion operator at (x_i, y_j) by

$$\nabla \cdot (A\nabla u^\epsilon) \Big|_{i,j} = \frac{\partial Q^{(1)}}{\partial x} \Big|_{i,j} + \frac{\partial Q^{(2)}}{\partial y} \Big|_{i,j} \approx \frac{Q_{i+1/2,j}^{(1)} - Q_{i-1/2,j}^{(1)}}{h_x} + \frac{Q_{i,j+1/2}^{(2)} - Q_{i,j-1/2}^{(2)}}{h_y} \tag{18}$$

with

$$Q_{i\pm 1/2,j} \approx A_{i\pm 1/2,j} \cdot \left(\frac{\partial u^\epsilon}{\partial x} \Big|_{i\pm 1/2,j}, \frac{\partial u^\epsilon}{\partial y} \Big|_{i\pm 1/2,j} \right)^T, \quad Q_{i,j\pm 1/2} \approx A_{i,j\pm 1/2} \cdot \left(\frac{\partial u^\epsilon}{\partial x} \Big|_{i,j\pm 1/2}, \frac{\partial u^\epsilon}{\partial y} \Big|_{i,j\pm 1/2} \right)^T.$$

The boundary values are given by the Dirichlet boundary conditions.

The major difference and difficulty is about discretization of the integration in the third equation in (14). The calculation is separated into two steps:

- Calculate $E(s)$. The quadrature points $\bar{p}_i (i = 0, 1, \dots, K_\ell)$ on each field line ℓ are determined as in section 3.1. We use the composite trapezoidal rule to approximate the integration in $E(s) = e^{\int_0^s \nabla \cdot \mathbf{b} \, ds'} + e^{-\int_{L_\ell}^s \nabla \cdot \mathbf{b} \, ds'}$. Since the discontinuities in $\nabla \cdot \mathbf{b}$ have been taken into account in the quadrature set, we calculate the value of $E(s)$ at the point p_k by

$$\exp \left(\sum_{i=0}^{k-1} \frac{\omega_i}{2} (\nabla \cdot \mathbf{b} \Big|_{\bar{p}_i} + \nabla \cdot \mathbf{b} \Big|_{\bar{p}_{i+1}}) \right) + \exp \left(- \sum_{i=k+1}^{K_\ell} \frac{\omega_{i-1}}{2} (\nabla \cdot \mathbf{b} \Big|_{\bar{p}_{i-1}} + \nabla \cdot \mathbf{b} \Big|_{\bar{p}_i}) \right). \tag{19}$$

Here $\omega_i = |\bar{p}_{i+1} - \bar{p}_i|$ is the Eulerian distance between the two quadrature points.

- The diffusion operator $-\nabla \cdot (\alpha \mathbf{b}_\perp (\mathbf{b}_\perp \cdot \nabla u^\epsilon))$ on each grid point is approximated by the centered finite difference method same as (18). Let S_1, S_2 be respectively the sets of quadrature points on the edge parallel to the x -axis and y -axis. The value of $\Theta = f + \nabla \cdot (\alpha \mathbf{b}_\perp (\mathbf{b}_\perp \cdot \nabla u^\epsilon))$ at the quadrature points p_k can be given by a linear interpolation such that:

$$\Theta \Big|_{\bar{p}_k} \approx \begin{cases} \Theta \Big|_{(x_i, y_j)} \frac{x_i + h_x - \bar{x}_i}{h_x} + \Theta \Big|_{(x_i + h_x, y_j)} \frac{\bar{x}_i - x_i}{h_x}, & \text{for } \bar{p}_k = (\bar{x}_i, y_j) \in S_1, \bar{x}_i \in (x_i, x_i + h_x), \\ \Theta \Big|_{(x_i, y_j)} \frac{y_j + h_y - \bar{y}_j}{h_y} + \Theta \Big|_{(x_i, y_j + h_y)} \frac{\bar{y}_j - y_j}{h_y}, & \text{for } \bar{p}_k = (x_i, \bar{y}_j) \in S_2, \bar{y}_j \in (y_j, y_j + h_y). \end{cases} \tag{20}$$

The integration in the third equation of (14) is approximated by

$$\sum_{i=0}^{K_\ell-1} \frac{\omega_i}{2} \left((E\Theta) \Big|_{\bar{p}_i} + (E\Theta) \Big|_{\bar{p}_{i+1}} \right) = 0, \tag{21}$$

with $\omega_i = |p_{i+1} - p_i|$.

For $\bar{p}_k = (x^*, y^*)$ inside the cell $[x_i, x_{i+1}] \times [y_j, y_{j+1}]$, $\Theta|_{\bar{p}_k}$ is given by the following bilinear interpolation $\Theta|_{\bar{p}_k} = \varpi_1 \Theta|_{(x_i, y_j)} + \varpi_2 \Theta|_{(x_{i+1}, y_j)} + \varpi_3 \Theta|_{(x_i, y_{j+1})} + \varpi_4 \Theta|_{(x_{i+1}, y_{j+1})}$ with

$$\begin{aligned}\varpi_1 &= \frac{(y_{j+1} - y^*)(x_{i+1} - x^*)}{h_x h_y}, & \varpi_2 &= \frac{(y_{j+1} - y^*)(x^* - x_i)}{h_x h_y}, \\ \varpi_3 &= \frac{(y^* - y_j)(x_{i+1} - x^*)}{h_x h_y}, & \varpi_4 &= \frac{(y^* - y_j)(x^* - x_i)}{h_x h_y}.\end{aligned}$$

4 Numerical Results

We present several tests to demonstrate the performance of the proposed scheme. For all examples, the precise discretizations in section 3 are used.

Example 1: In this example, the following exact solution for $(x, y) \in [-0.5, 0.5] \times [-0.5, 0.5]$ is considered:

$$u(x, y) = 1 - [\gamma_1^2(x \cos \varphi + y \sin \varphi)^2 + \gamma_2^2(x \sin \varphi - y \cos \varphi)^2]^{3/2}. \quad (22)$$

We test four different choices of γ_1 , γ_2 and φ . All cases include closed field lines (see Figure 4). In the first two cases, the closed field lines are ellipses that are symmetric with respect to the x and y axes, while in the last two cases, the ellipses are rotated.

For the first symmetric cases, there exist schemes in the literature [8, 10, 11] that exhibit uniform second order convergence with respect to ϵ . However, when the closed field lines become tilted ellipses, the convergence order of all schemes discussed in [8, 10, 11] depends on the level of anisotropy. In particular, when ϵ reaches the order of 10^{-9} , no convergence can be observed with $h_x, h_y \gg \epsilon$ in the tilted ellipse case.

The field and diffusion tensor are given by

$$\mathbf{b} = \frac{1}{\sqrt{u_x^2 + u_y^2}} \begin{pmatrix} -u_y \\ u_x \end{pmatrix} = \begin{pmatrix} b_1 \\ b_2 \end{pmatrix}, \quad A = \begin{pmatrix} b_1 & -b_2 \\ b_2 & b_1 \end{pmatrix} \begin{pmatrix} 1/\epsilon & 0 \\ 0 & 1 \end{pmatrix} \begin{pmatrix} b_1 & b_2 \\ -b_2 & b_1 \end{pmatrix},$$

while the boundary conditions and the source term are determined by substituting the exact solutions into (1). At the origin (0,0), b has no definition. We replace $\sqrt{u_x^2 + u_y^2}$ by $\sqrt{u_x^2 + u_y^2 + \delta}$ ($\delta = O(10^{-16})$) to approximate the solution at the origin.

In the first case, $\nabla \cdot \mathbf{b} = 0$ on each field line. In all other cases, $\nabla \cdot \mathbf{b} \neq 0$, and the discontinuities of $\nabla \cdot \mathbf{b}$ are distributed on a ray. The angle between the ray and the x -axis is equal to φ , as shown in Figure 5.

Convergence Order The convergence orders of our new scheme are displayed in Figure 6. Second order convergence in both L^2 and L^∞ norm can be observed regardless of the anisotropy strength. Figure 8 (a) shows that, when ϵ is less than the order of 10^{-3} , the numerical errors by the classical 9-Point FDM of the original system (1) does not decrease as the mesh is refined. When the closed field lines become tilted ellipses, the convergence order of all schemes discussed in [8, 10, 11] depends on the level of anisotropy. The comparison illustrates the advantage of our reformulation.

Condition Number The condition numbers of four cases are displayed on Figure 7, it is shown that the condition number of the discretized system is bounded by a constant independent of ϵ that has the same magnitude as the classical 9-Point FDM, see Figure 8 (b). However, [18] has pointed out that numerical discretizations of the original problem using magnetic field aligned coordinates lead to very badly conditioned systems when ϵ becomes small.

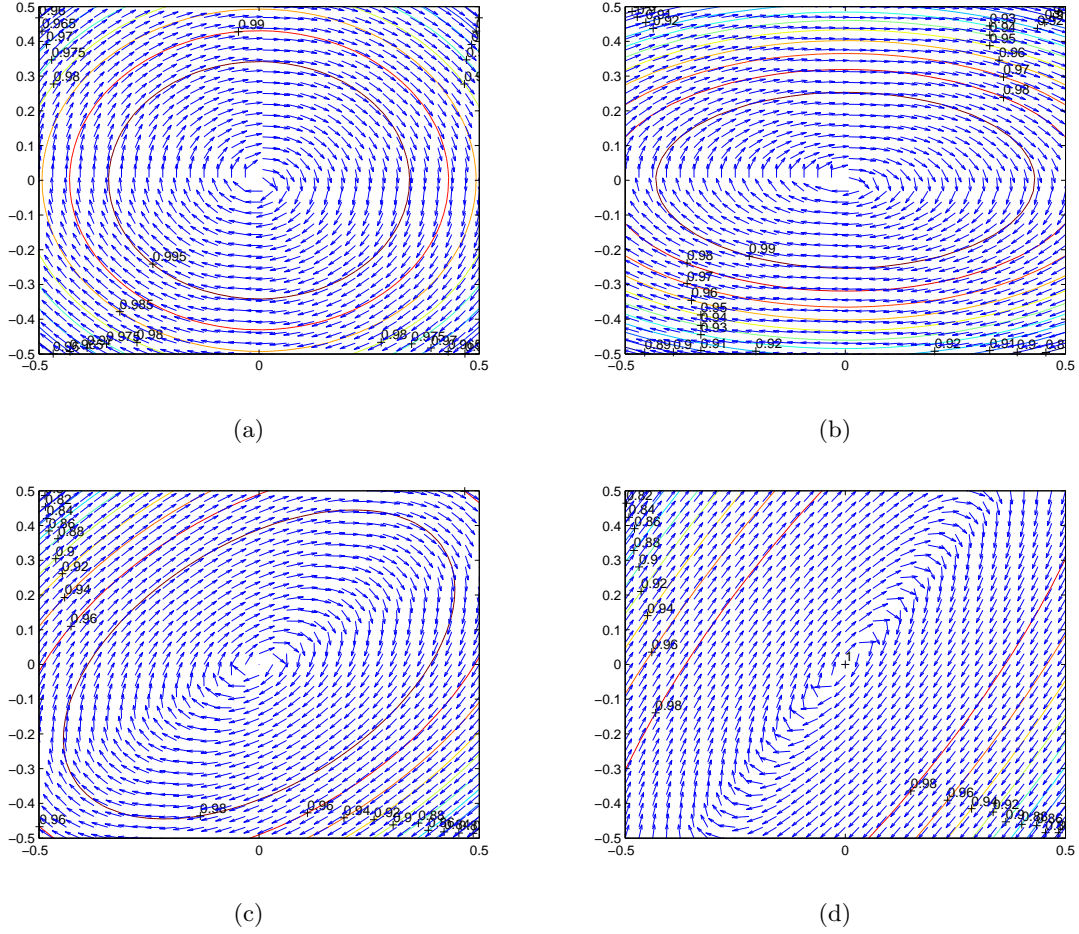


Figure 4: Example 1. The fields of the four test cases. (a). $\gamma_1 = \gamma_2 = 0.5$, $\varphi = 0$. (b). $\gamma_1 = 0.5$, $\gamma_2 = 0.85$, $\varphi = 0$. (c). $\gamma_1 = 0.5$, $\gamma_2 = 0.85$, $\varphi = \pi/4$. (d). $\gamma_1 = 0.25$, $\gamma_2 = 0.85$, $\varphi = \pi/3$.

As discussed in section 3.1, the closed field lines can be numerically determined in two different ways. We illustrate here that it is important to use "Method Two", in order to get uniform second order convergence. Take $\gamma_1 = 0.5$, $\gamma_2 = 0.85$ and $\theta = \pi/4$ in (22) as an example. The results are displayed in Figure 9 and no uniform convergence can be observed for "Method One", while "Method Two" works quite well.

Example 2: We consider the case when there exhibit two "magnetic islands". Let the computational domain be $[-1, 1] \times [-0.5, 0.5]$ and exact solution be

$$u_{exact}^\epsilon = \cos(\lambda \cos(2\pi(x - 3/2)) + \cos(\pi y)) + \epsilon \sin(2\pi y) \sin(\pi x). \quad (23)$$

As $\epsilon \rightarrow 0$, u_{exact}^ϵ converges to $u^0 = \cos(\lambda \cos(2\pi(x - 3/2)) + \cos(\pi y))$. Let

$$\mathbf{b} = \frac{B}{|B|}, \quad B = \begin{pmatrix} -\pi \sin(\pi y) \\ \lambda 2\pi \sin(2\pi(x - 3/2)) \end{pmatrix} = \begin{pmatrix} B_1 \\ B_2 \end{pmatrix}. \quad (24)$$

Then \mathbf{b} satisfies $\mathbf{b} \cdot \nabla u^0 = 0$, which indicates that the limiting solution u^0 is a constant along the field line. This is how we construct \mathbf{b} .

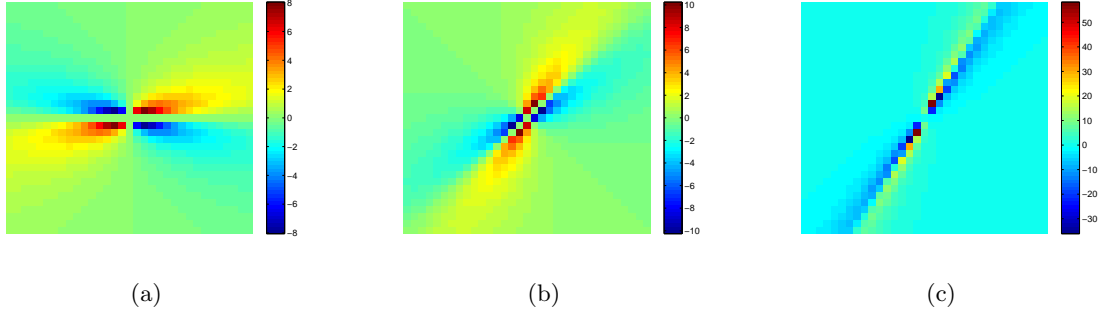


Figure 5: Example 1. $\nabla \cdot \mathbf{b}$, $I \times J = 32 \times 32$. (a). $\gamma_1 = 0.5$, $\gamma_2 = 0.85$, $\varphi = 0$. (b). $\gamma_1 = 0.5$, $\gamma_2 = 0.85$, $\varphi = \pi/4$. (c). $\gamma_1 = 0.25$, $\gamma_2 = 0.85$, $\varphi = \pi/3$.

The source term is calculated by plugging (23), (24) into (1). The field is showed in Figure 10 (a). In this example, \mathbf{b} has no definition at five points: $(-1, 0)$, $(-0.5, 0)$, $(0, 0)$, $(0.5, 0)$, $(1, 0)$ and $\nabla \cdot \mathbf{b}$ change quickly near these points (see Figure 10 (b)). Two of these five singular points $(-0.5, 0)$ and $(0.5, 0)$ are the centers of the “magnetic island”, while the other three are the connection points of two “magnetic islands”. $\sqrt{B_1^2 + B_2^2 + \delta}$ ($\delta = 10^{-16}$) are used to replace $\sqrt{B_1^2 + B_2^2}$, in order to approximate the values at the five singular points. The convergence order of our scheme is around $1.5 \sim 1.6$ for ϵ ranging from 10^{-12} to 10^{-3} (See Figure 10 (c), (d)). This is caused by the three singular points of \mathbf{b} at $(-1, 0)$, $(0, 0)$, $(1, 0)$.

5 Conclusion

We present a simple Asymptotic-Preserving formulation for strongly anisotropic diffusion equation with closed field lines. The key idea is that we cut each of the closed field line at some point (x_0, y_0) and replace locally discretizing the equation at the point (x_0, y_0) by integration of the differential equation along the cut field line so that the singular $1/\epsilon$ terms disappear. The new system removes the ill-posedness and uniform second order convergence with respect to the anisotropy is observed numerically, even for the tilted ellipse case.

The scheme is efficient, general and easy to implement. The idea can be coupled with most standard discretizations and the computational cost keeps almost the same. Only slight modification to the original code is required, which makes it attractable to engineers.

Acknowledgement

This work was partially supported by NSFC 11301336 and 91330203. The authors would like to thank Professor Chunjing Xie for his valuable suggestions.

References

- [1] D. N. Arnold, An interior penalty finite element method with discontinuous elements, SIAM J. Numer. Anal. 19 (4) (1982) 742-760.

- [2] S. F. Ashby, W.J. Bosl, R.D. Falgout, S.G. Smith, A.F. Thompson, T.J. Williams, A numerical simulation of groundwater flow and contaminant transport on the CRAY T3D and C90 Supercomputers, *International Journal of High Performance Computing Applications* 13 (1) (1999) 80-93.
- [3] P. Degond, F. Deluzet, C. Negulescu, An asymptotic preserving scheme for strongly anisotropic elliptic problems, *Multiscale Model. Simul.* 8 (2) (2010) 645-666.
- [4] P. Degond, F. Deluzet, L. Navoret, A. B. Sun, M. Vignal, Asymptotic-Preserving Particle-In-Cell method for the Vlasov-Poisson system near quasineutrality, *J. Comput. Phys.* 229 (16) (2010) 5630-5652.
- [5] P. Degond, A. Lozinski, J. Narski, C. Negulescu, An Asymptotic-Preserving method for highly anisotropic elliptic equations based on a micro-macro decomposition, *J. Comput. Phys.* 231 (7) (2012) 2724-2740.
- [6] P. Degond, F. Deluzet, A. Lozinski, J. Narski, C. Negulescu, Duality-based Asymptotic-Preserving method for highly anisotropic diffusion equations, *Commun. Math. Sci.* 10 (2012) 1-31.
- [7] A. Ern, A. F. Stephansen, P. Zunino, A discontinuous Galerkin method with weighted averages for advection-diffusion equations with locally small and anisotropic diffusivity, *IMA J. Numer. Anal.* 29 (2) (2009) 235-256.
- [8] B. van Esa, B. Koren, H. J. de Blank, Finite-difference schemes for anisotropic diffusion, *J. Comput. Phys.* 272 (1) (2014) 526-549.
- [9] B. Galperin, S. Sukoriansky, Geophysical flows with anisotropic turbulence and dispersive waves: flows with stable stratification, *Ocean Dynamics* 60 (5) (2010) 1319-1337.
- [10] S. Günter, K. Lackner, C. Tichmann, Finite element and higher order difference formulations for modeling heat transport in magnetized plasmas, *J. Comput. Phys.* 226 (2) (2007) 2306-2316.
- [11] S. Günter, Q. Yu, J. Krüer, K. Lackner, Modelling of heat transport in magnetized plasmas using non-aligned coordinates, *J. Comput. Phys.* 209 (1) (2005) 354-370.
- [12] R. Herbin, F. Hubert, Benchmark on Discretization Schemes for Anisotropic Diffusion Problems on General Grids, *Finite volumes for complex applications V*, France (2008).
- [13] T. Y. Hou, X. H. Wu, A Multiscale Finite Element Method for Elliptic Problems in Composite Materials and Porous Media, *J. Comput Phys.* 134 (1) (1997) 169-189.
- [14] J. Hyman, J. Morel, M. Shashkov, S. Steinberg, Mimetic finite difference methods for diffusion equations, *Computational Geosciences* 6 (3) (2002) 333-352.
- [15] X. Li, W. Huang, An anisotropic mesh adaptation method for the finite element solution of heterogeneous anisotropic diffusion problems, *J. Comput. Phys.* 229 (21) (2010) 8072-8094.
- [16] A. Lozinski, J. Narski, C. Negulescu, Highly anisotropic temperature balance equation and its asymptotic-preserving resolution, *ESAIM: Mathematical Modelling and Numerical Analysis* 48 (6) (2014) 1701-1724.

- [17] A. Mentrelli, C. Negulescu, Asymptotic-preserving scheme for highly anisotropic non-linear diffusion equations, *J. Comput. Phys.* 231 (24) (2012) 8229-8245.
- [18] J. Narski, M. Ottaviani, Asymptotic preserving scheme for strongly anisotropic parabolic equations for arbitrary anisotropy direction. *Computer Physics Communications* 185 (2014) 3189-3203.
- [19] J. Pasdunkorale, I. W. Turner, A second order control-volume finite-element least-squares strategy for simulating diffusion in strongly anisotropic media, *J Comput. Math.* 23 (1) (2005) 1-16.
- [20] C. L. Potier, A finite volume method for the approximation of highly anisotropic diffusion operators on unstructured meshes, in *Finite Volumes for Complex Applications IV*, 2005.
- [21] Z. Q. Sheng, J. Y. Yue, G. W. Yuan, Monotone finite volume schemes of nonequilibrium radiation diffusion equations on distorted meshes, *SIAM J. Sci. Comput.* 31 (4) (2009) 2915-2934.
- [22] A. M. Treguier. Modelisation numerique pour loceanographie physique, *Ann. Math. Blaise Pascal.* 9 (2) (2002) 345-361.
- [23] M. Tang, Y. H. Wang, An Asymptotic Preserving method for strongly anisotropic diffusion equations based on field line integration, arXiv:1608.00541, submitted (review back with minor revision).
- [24] G. W. Yuan, Z. Q. Sheng, Monotone finite volume schemes for diffusion equations on polygonal meshes, *J. Comput. Phys.* 227 (12) (2008) 6288-6312.

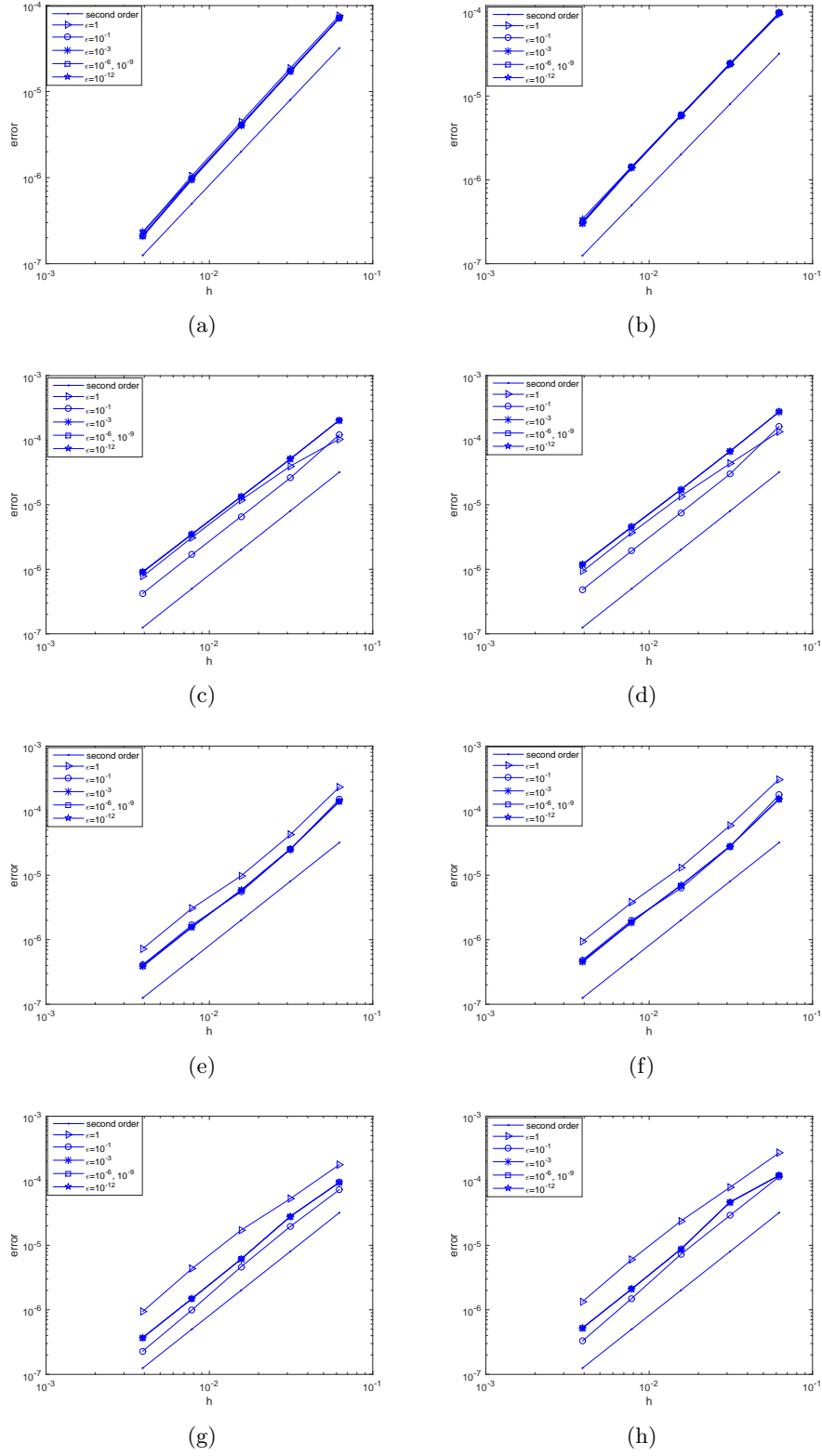
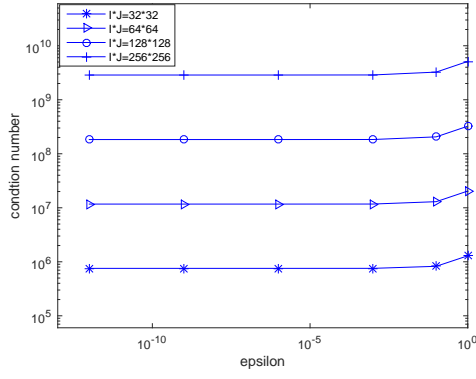
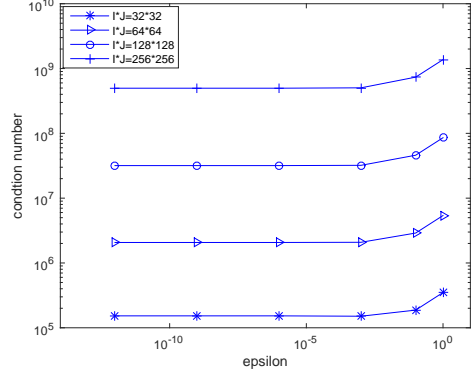


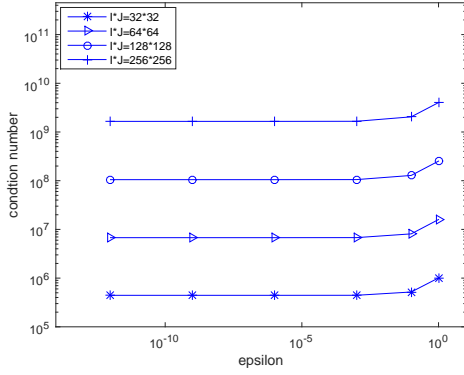
Figure 6: Example 1. Convergence orders for L^2 error (Left) and L^∞ error (Right). (a). (b). $\gamma_1 = \gamma_2 = 0.5$, $\varphi = 0$. (c). (d). $\gamma_1 = 0.5$, $\gamma_2 = 0.85$, $\varphi = 0$. (e). (f). $\gamma_1 = 0.5$, $\gamma_2 = 0.85$, $\varphi = \pi/4$. (g). (h). $\gamma_1 = 0.25$, $\gamma_2 = 0.85$, $\varphi = \pi/3$.



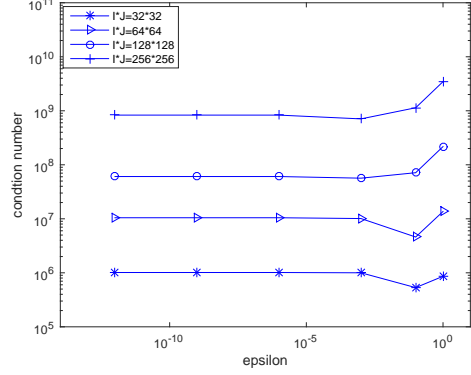
(a)



(b)

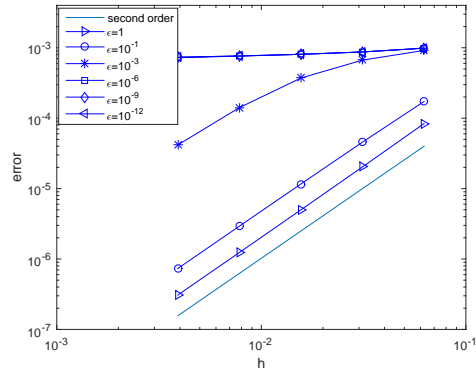


(c)

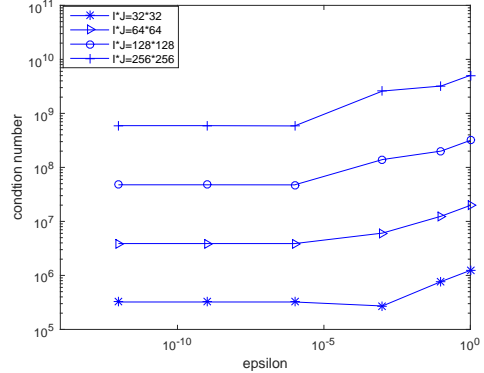


(d)

Figure 7: Example 1. The condition number for different grids and different ϵ values. (a). $\gamma_1 = \gamma_2 = 0.5$, $\varphi = 0$. (b). $\gamma_1 = 0.5$, $\gamma_2 = 0.85$, $\varphi = \pi/4$. (c). $\gamma_1 = 0.25$, $\gamma_2 = 0.85$, $\varphi = \pi/3$.

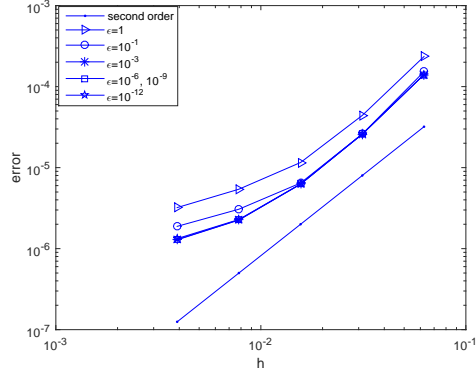


(a)

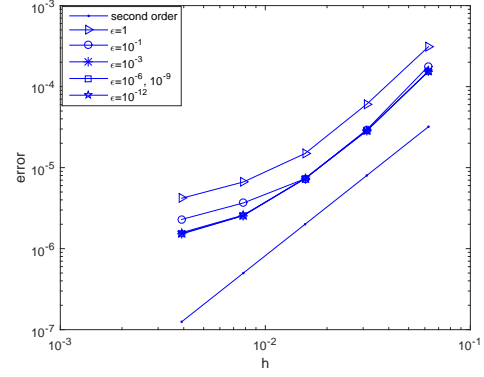


(b)

Figure 8: Example 1. $\gamma_1 = 0.5$, $\gamma_2 = 0.5$, $\varphi = 0$. Convergence orders for L^∞ error and Condition number estimate for the classical 9-point FDM. (a). Convergence orders. (b). Condition number.

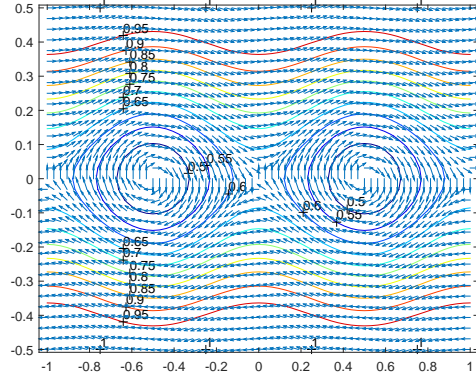


(a)

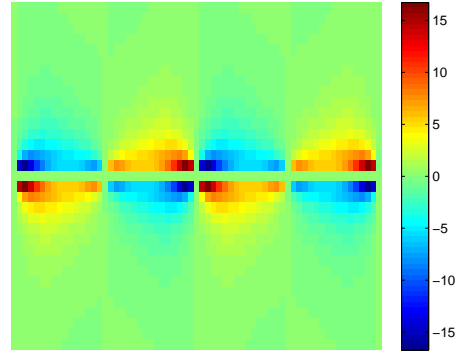


(b)

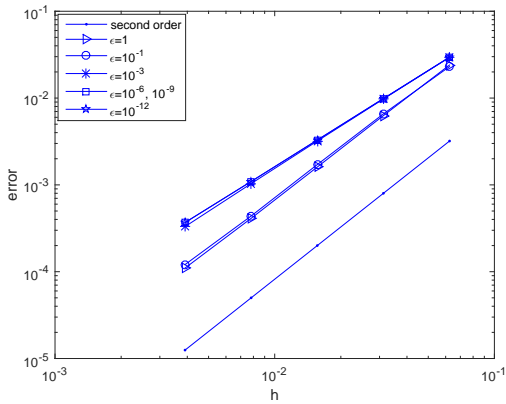
Figure 9: Example 1. $\gamma_1 = 0.5$, $\gamma_2 = 0.85$, $\varphi = \pi/4$. Convergence orders based on the closed field line is solved by "Method One". (a). Convergence orders for L^2 error. (b). Convergence orders for L^∞ error.



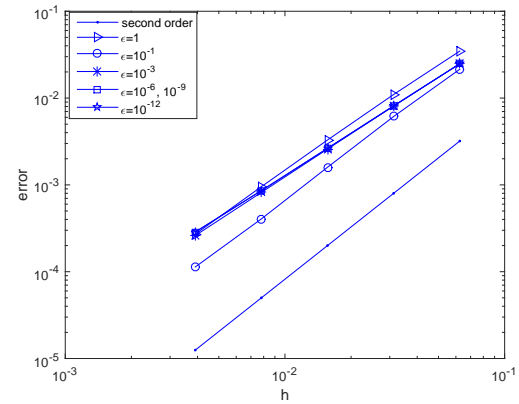
(a)



(b)



(c)



(d)

Figure 10: Example 2. $\lambda = 0.1$. (a). Closed field. (b). $\nabla \cdot \mathbf{b}$, $I \times J = 64 \times 32$. (c). Convergence orders for L^2 error. (d). Convergence orders for L^∞ error.